Investigation of secondary γ-ray angular distributions using the $^{15}\mathrm{N}(p,\alpha_1\gamma)\,^{12}\mathrm{C}^*$ reaction

R. J. deBoer,[*] A. Boeltzig,[†] K. T. Macon,[‡] S. Aguilar, O. Gomez, B. Frentz, S. L. Henderson, R. Kelmar, M. Renaud, G. Seymour,[§] B. Vande Kolk, and M. Wiescher
The Joint Institute for Nuclear Astrophysics, Department of Physics, University of Notre Dame, Notre Dame, Indiana 46556, USA

C. R. Brune
Edwards Accelerator Laboratory, Department of Physics and Astronomy, Ohio University, Athens, Ohio 45701, USA

S. P. Burcher, K. L. Jones, and J. M. Kovoor
Department of Physics and Astronomy, University of Tennessee, Knoxville, Tennessee 37996, USA

M. Febbraro
Oak Ridge National Laboratory, Oak Ridge, Tennessee 37830, USA

G. Imbriani
Università degli Studi di Napoli "Federico II", Dipartimento di Fisica E. Pancini, Via Cintia 21, 80126 Napoli, and INFN, Naples, Italy

S. Mosby
P-27: Los Alamos National Laboratory, Mailstop H805, Los Alamos, New Mexico 87545, USA

K. Smith
Los Alamos National Laboratory, Los Alamos, New Mexico 87545, USA

R. Toomey
Department of Physics and Astronomy, Rutgers University, New Brunswick, New Jersey 08901, USA

(Received 12 June 2020; revised 11 May 2021; accepted 1 June 2021; published 14 June 2021)

The observation of secondary γ-rays provides an alternative method of measuring cross sections that populate excited final states in nuclear reactions. The angular distributions of these γ-rays also provide information on the underlying reaction mechanism. Despite the large number of data of this type in the literature, publicly available R-matrix codes do not have the ability to calculate these types of angular distributions. In this paper, the mathematical formalism derived by C. R. Brune and R. J. deBoer [Phys. Rev. C **102**, 024628 (2020)] is implemented in the R-matrix code AZURE2 and calculations are compared with previous data from the literature for the $^{15}\mathrm{N}(p,\alpha_1\gamma)\,^{12}\mathrm{C}^*$ reaction. In addition, new measurements, made at the University of Notre Dame Nuclear Science Laboratory using the Hybrid Array of Gamma Ray Detectors (HAGRiD), are reported that span the energy range from $E_p = 0.88$ MeV to $E_p = 4.0$ MeV. Excellent agreement between the data and the phenomenological fit is obtained up to the limit of the previous fit at $E_p = 2.0$ MeV and the R-matrix fit is extended from $E_x \approx 13.5$ MeV up to $E_x \approx 15.3$ MeV, where $^{15}\mathrm{N}+p$ and $^{12}\mathrm{C}+\alpha$ reactions are fit simultaneously for the first time. An excellent reproduction of the $^{15}\mathrm{N}(p,\alpha_1\gamma)\,^{12}\mathrm{C}^*$ and $^{12}\mathrm{C}(\alpha,\alpha)\,^{12}\mathrm{C}$ data is achieved, but inconsistencies and difficulty in fitting other data are encountered and discussed.

DOI: 10.1103/PhysRevC.103.065801

I. INTRODUCTION

For reactions that populate excited states in the final nucleus, measurements of secondary γ-rays often provide an alternative method of determining the cross section in place of measurements of the promptly emitted particles. The method has a variety of experimental advantages. For instance, the energy resolution of high-purity germanium detectors is often better than that of a standard surface barrier detector, providing improved spectroscopic resolution. Since γ-rays usually

[*]rdeboer1@nd.edu
[†]Present address: Gran Sasso National Laboratory (LNGS), Via G. Acitelli 22, 67100 Assergi (AQ), Italy.
[‡]Present address: Department of Physics and Astronomy, Louisiana State University, Baton Rouge, Louisiana 70803, USA.
[§]Present address: Department of Physics, Rutgers University, Piscataway, New Jersey 08854, USA.

suffer only moderate attenuation through typical beamline components, their measurement is less dependent on the experimental setup geometry and is easier to calibrate and model than for neutrons. Further, since the secondary γ-ray energy is fixed, the efficiency is independent of the beam energy and the efficiency can be determined readily with radioactive sources or well-known reactions. This is also useful when studying reactions near their thresholds. These types of measurements are useful for a variety of applications, from nuclear astrophysics and nuclear structure studies to ion beam analysis and neutron interrogation.

There is already a large number of data of this type available in the literature, yet no *R*-matrix code has the capability to calculate the angular distributions of secondary γ-rays. To remedy this situation, the theory has recently been derived by Brune and deBoer [1] and implemented in the *R*-matrix code AZURE2 [2,3]. Initial comparison calculations were made to those of Bray *et al.* [4] for the reaction $^{15}\mathrm{N}(p,\alpha_1\gamma)\,^{12}\mathrm{C}^*$. This work expands on that analysis with new measurements of the $^{15}\mathrm{N}(p,\alpha_1\gamma)\,^{12}\mathrm{C}^*$ reaction and work towards expanding the *R*-matrix fit of the ^{16}O system to higher energies. This study was also motivated by an international effort by the Nuclear Data Section of the International Atomic Energy Agency (IAEA) to produce expanded and more accurate evaluated cross sections of charged-particle-induced reactions for ion beam analysis (IBA) and other applications [5–8]. Reaction studies that utilize secondary γ-rays are a critical part of this effort.

The $^{15}\mathrm{N}(p,\alpha_1\gamma)\,^{12}\mathrm{C}^*$ reaction has been chosen for study and analysis because of the availability of previous literature data and *R*-matrix analyses to compare against [9,10]. The reaction has seen several past measurements because the $^{15}\mathrm{N}(p,\alpha)\,^{12}\mathrm{C}$, $^{15}\mathrm{N}(p,\gamma)\,^{16}\mathrm{O}$, and $^{12}\mathrm{C}(\alpha,\gamma)\,^{16}\mathrm{O}$ reactions, which often populate levels in the ^{16}O compound system, are all key reactions in nuclear astrophysics. Further, the $^{15}\mathrm{N}(p,\alpha_1\gamma)\,^{12}\mathrm{C}^*$ reaction is commonly used in IBA to study the properties of thin films containing either nitrogen, using low-energy proton beams (see, for example, Hirvonen *et al.* [11] and Kumar *et al.* [12]), or hydrogen, using ^{15}N ion beams (see, for example, Lanford [13], Krauser *et al.* [14], Wilde and Fukutani [15]).

deBoer *et al.* [10] showed that a multichannel *R*-matrix analysis of the ^{16}O system can give greatly improved constraints on all of the reactions that populate the compound system through improved understanding of the contributions to the cross section. The analysis was then expanded to evaluate the $^{12}\mathrm{C}(\alpha,\gamma)\,^{16}\mathrm{O}$ reaction [16]. Angular distributions of secondary γ-rays provide yet another useful set of data to constrain the phenomenological description of the compound system. Here this global analysis is expanded to included both the $^{15}\mathrm{N}(p,\alpha_1\gamma)\,^{12}\mathrm{C}^*$ and the $^{12}\mathrm{C}(\alpha,\alpha_1\gamma)\,^{12}\mathrm{C}$ reactions.

In Sec. II the differential cross section for reactions producing secondary γ-rays is described in the *R*-matrix framework. Section II B compares the results of previous $^{15}\mathrm{N}(p,\alpha_1\gamma)\,^{12}\mathrm{C}^*$ measurements with a previously published *R*-matrix analysis in which no $^{15}\mathrm{N}(p,\alpha_1\gamma)\,^{12}\mathrm{C}^*$ data were considered. New experimental measurements are presented in Sec. III and a review of past data is given in Sec. IV. An extension of the previous *R*-matrix analysis is described in Sec. V and a summary is given in Sec. VII.

II. *R*-MATRIX IMPLEMENTATION OF SECONDARY γ-RAY ANGULAR DISTRIBUTIONS

In this section the pertinent formalism derived by Brune and deBoer [1] is summarized and the comparison to previous measurements of the $^{15}\mathrm{N}(p,\alpha_1\gamma)\,^{12}\mathrm{C}^*$ reaction is expanded.

A. *R*-matrix formalism

The derivation of the differential cross section for secondary γ-ray emission has been given by Brune and deBoer [1]. Only those formulas that have been directly implemented in the AZURE2 [2,3] *R*-matrix code are repeated here.

Following the notation of Lane and Thomas [17], the differential cross section for secondary γ-ray emission for a two-body reaction of the type $A(a,b)B$ followed by the decay $B\rightarrow C+\gamma$ can be written as

$$\frac{d\sigma}{d\Omega_\gamma}=\frac{1}{(2I_A+1)(2I_a+1)}\frac{\pi}{k_{aA}^2}\times\sum_k(2k+1)^{1/2}R_k(\gamma)\frac{P_k(\cos\theta_\gamma)}{4\pi}H_k,\qquad(1)$$

where

$$\begin{aligned}H_k=&\sum_{J_1J_2\ell_1\ell_2\ell's s_1's_2'}(-1)^{k+s_2'-s_1'}(2J_1+1)(2J_2+1)\\&\times[(2\ell_1+1)(2I_B+1)(2s_1'+1)(2s_2'+1)]^{1/2}\\&\times(k\ell_100|\ell_20)\,W(kI_Bs_2'I_b;I_Bs_1')\\&\times W(ks_1'J_2\ell';s_2'J_1)\,W(kJ_1\ell_2s;J_2\ell_1)\\&\times T^{J_1*}_{bBs_1'\ell':aAs\ell_1}T^{J_2}_{bBs_2'\ell':aAs\ell_2},\end{aligned}\qquad(2)$$

giving a form analogous to the reaction portion of the differential cross-section formula given by Eq. (VIII, 2.4) of Lane and Thomas [17]. Here I_x denotes the intrinsic spin of nuclear state X, ℓ are relative angular momenta, s are channel spins, J are total spins, $T^{J_1*}_{bBs_1'\ell':aAs\ell_1}$ and $T^{J_2}_{bBs_2'\ell':aAs\ell_2}$ are elements of the transition matrix, $(k\ell_100|\ell_20)$ is a Clebsch-Gordan coefficient, and $W(kI_Bs_2'I_b;I_Bs_1')$, $W(ks_1'J_2\ell';s_2'J_1)$, and $W(kJ_1\ell_2s;J_2\ell_1)$ are Racah coefficients. The γ radiation parameters $R_k(\gamma)$ are given by [18,19]

$$R_k(\gamma)=\sum_{LL'}g_L\,g_{L'}\,R_k(LL'I_BI_C),\qquad(3)$$

where

$$\begin{aligned}R_k(LL'I_BI_C)=&(2I_B+1)^{1/2}(2L+1)^{1/2}(2L'+1)^{1/2}\\&\times(-1)^{I_B-I_C+L-L'+k+1}(L'L1-1|k0)\\&\times W(LL'I_BI_B;kI_C).\end{aligned}\qquad(4)$$

Here, L and L' take on the values of the multipolarities of the possible γ-ray transitions. The amplitudes g_L describe the relative strengths of the multipoles. Note that $R_0=1$ and parity considerations require that k only take on even values,

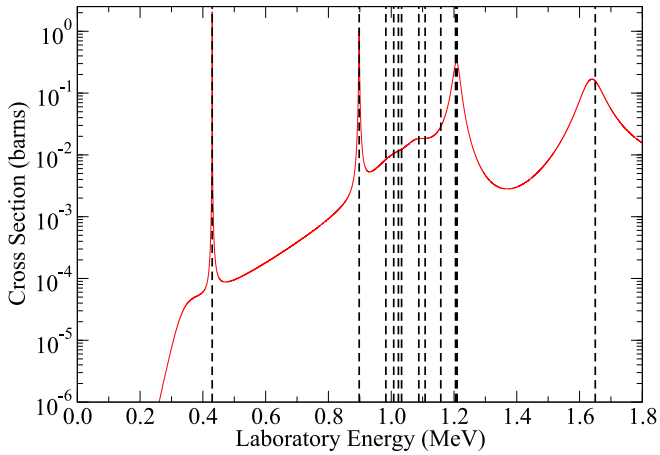

FIG. 1. The solid red line indicates an R-matrix calculation of the angle-integrated $^{15}\mathrm{N}(p,\alpha_1\gamma)\,^{12}\mathrm{C}^*$ cross section using the level parameters reported by deBoer *et al.* [16]. The differential cross-section measurements of Bray *et al.* [4] are the only ones made in off-resonance regions. The energies of these measurements are indicated by the dashed vertical lines.

but note that Eq. (4) is not necessarily 0 for odd values of k (see the footnote in Ref. [18]).

It is often the case that only the first two multipoles are significant or that this assumption is a good approximation. In this situation, the sums over L and L' are limited to L and $L+1$ and Eq. (3) reduces to [19]

$$R_k(\gamma) = [R_k(LLI_BI_C) + 2\delta R_k(LL+1I_BI_C) + \delta^2 R_k(L+1L+1I_BI_C)]/(1+\delta^2), \quad (5)$$

where δ is the multipole branching ratio. If only one multipole dominates the transition, Eqs. (3) and (4) reduce further to

$$R_k(\gamma) = (2I_B+1)^{1/2}(2L+1)(-1)^{I_B-I_C+k+1} \times (LL1-1|k0)\,W(LLI_BI_B;kI_C). \quad (6)$$

This is the situation for the $^{15}\mathrm{N}(p,\alpha_1\gamma)\,^{12}\mathrm{C}^*$ and $^{12}\mathrm{C}(\alpha,\alpha_1\gamma)\,^{12}\mathrm{C}^*$ reactions analyzed in this work.

B. Benchmark calculations to previous measurements

deBoer *et al.* [10] performed a comprehensive R-matrix fit of the $^{16}\mathrm{O}$ compound system up to $E_x \approx 13.75$ MeV. The R-matrix fit was made using a wide variety of reaction data but did not utilize any secondary γ-ray differential cross-section data for the $^{15}\mathrm{N}(p,\alpha_1\gamma)\,^{12}\mathrm{C}^*$ reaction. The updated set of R-matrix parameters is given in Table XXI of deBoer *et al.* [16] and can also be found in the AZURE2 input file provided in the Supplemental Material of that work.

There are several measurements of the low-energy cross section of the $^{15}\mathrm{N}(p,\alpha_1\gamma)\,^{12}\mathrm{C}^*$ reaction, however, most of these measurements focus on the strong $E_p = 429$ and 897 keV resonances [4,20–22]. Only Bray *et al.* [4] make off-resonance measurements. Figure 1 shows the angle-integrated $^{15}\mathrm{N}(p,\alpha_1\gamma)\,^{12}\mathrm{C}^*$ cross section as a function of the energy from deBoer *et al.* [10], where the dashed lines indicate the previous angular distribution measurements by Bray *et al.* [4]. A comparison of these cross sections with the R-matrix cross section calculated with the parameters from deBoer *et al.* [16] and using the formalism described in Sec. II A are shown in Fig. 2. No further fitting has been performed. The R-matrix parameters for the levels that correspond to broad resonances in the cross section were determined previously through a simultaneous fit to all allowed reaction channels in this excitation energy region in $^{16}\mathrm{O}$. The R-matrix parameters for the 2^- levels that correspond to the two narrow resonances in the $^{15}\mathrm{N}(p,\alpha_1\gamma)\,^{12}\mathrm{C}^*$ at $E_p = 429$ and 897 keV were not determined through fitting but were instead taken from the analysis by Leavitt *et al.* [23]. In order to reproduce the previous data it is also important to correct for the finite detector size for each experiment. The effect of the detector geometry is most significant for the data measured at the $E_p = 429$ and 897 keV resonances, as these angular distributions change rapidly with angle. The geometric correction is given in terms of Q coefficients Q_k, which act as correction factors to the angular distribution coefficients a_k in a Legendre polynomial $P_k(\cos(\theta))$ expansion of the differential cross section

$$W(\theta) = \sum_{k=0}^{k_{\max}} a_k Q_k P_k(\cos(\theta)), \quad (7)$$

where θ is the angle defining the angle between the incoming beam and the emitted γ-ray [24]. Since the reactions under investigation are at low energy, the approximation is made that the laboratory and center-of-mass angle of the observed γ-ray are equivalent. This approximation is estimated to be accurate to better than 3% for all kinematic configurations relevant to this work. The Q coefficients for the previous measurements are listed in Table I. Since secondary γ-ray angular distributions are symmetric about 90°, the summation in Eq. (7) reduces to only the even terms in k.

TABLE I. Q coefficients. Since the differential cross sections of secondary γ-ray angular distributions are symmetric about 90°, only even terms are necessary. Because the data are limited to low energies, only $L \leqslant 4$ terms are considered.

Reference	Q_2	Q_4
Kraus *et al.* [20]	0.955	0.857
Barnes *et al.* [21]	0.8	0.6
Bashkin and Carlson [22]	0.8	0.6
Bray *et al.* [4]	0.85	0.7
This work	0.999	0.994

III. MEASUREMENTS OF THE $^{15}\mathrm{N}(p,\alpha_1\gamma)\,^{12}\mathrm{C}^*$ REACTION

Measurements were performed in order to expand the scope of the previous data from the literature described in Sec. II B as well as to expand the amount of measurements at energies up to $E_p = 4.0$ MeV.

Measurements were made at the University of Notre Dame Nuclear Science Laboratory using the 5-MV Santa Ana accelerator to produce proton beams over the range of $E_p = 0.88$ to 4.0 MeV with intensities of up to 15 μA on the target. The beam energy has been calibrated using the well-known

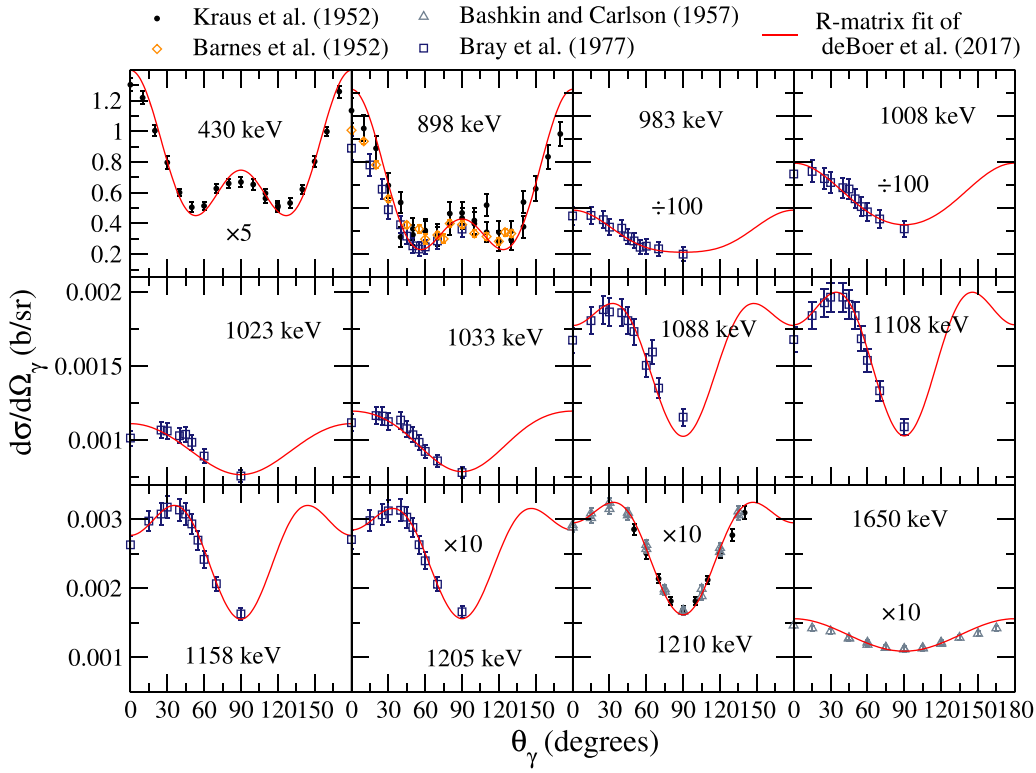

FIG. 2. All known angular distribution measurements of the $^{15}\mathrm{N}(p,\alpha_1\gamma)\,^{12}\mathrm{C}^*$ cross section over the region from threshold up to $E_p \approx 2$ MeV. The measurements by Bray *et al.* [4] are the only ones made in off-resonance regions. The solid red line indicates an *R*-matrix calculation using the level parameters reported by deBoer *et al.* [16], which are in good agreement with the data.

narrow resonance in the $^{27}\mathrm{Al}(p,\gamma)\,^{28}\mathrm{Si}$ reaction at $E_p = 992$ keV [25] and has been found to be reproducible to ± 1 keV with an energy spread of 0.3 keV full width at half-maximum. The beam was impinged on a thin titanium nitride target that was produced by reactive sputtering on a thick Ta backing. The target was enriched in $^{15}\mathrm{N}$ to 99.95 at% and had a stoichiometry of 1:1 (with an uncertainty of 2%). The target backing was water-cooled to mitigate deterioration due to beam heating. An electrically isolated, liquid-nitrogen-cooled, copper pipe biased to -300 V was used both as a cold trap and for secondary electron suppression.

The Ti $^{15}\mathrm{N}$ target was nearly identical to that used previously for the $^{15}\mathrm{N}(p,\gamma)\,^{16}\mathrm{O}$ measurements reported by LeBlanc *et al.* [26] and Imbriani *et al.* [27] and had an effective thickness of 3.7(2) keV at $E_p = 897$ keV. Target stability was verified in the present measurements by repeating the thick target yield scan over the narrow resonance at $E_p = 897$ keV throughout the measurements. Due to the relatively large cross section over this energy region, less than 0.3 C of charge was accumulated on the target. No degradation of the targets was observed over the course of the experiment. This is expected since LeBlanc *et al.* [26] reported that 5 C of charge was accumulated at higher beam intensities and no degradation was found.

The 4.44-MeV γ-rays from the decay of the first excited state of $^{12}\mathrm{C}$ were detected using the Hybrid Array of Gamma Ray Detectors (HAGRiD) [28], a set of 2 in. thick × 2 in. diameter $LaBr_3$(Ce) detectors. The detectors were placed in a far geometry, $\approx$ 12 in. from the target, to limit the effects of finite solid angle coverage. The setup is shown in Figs. 3 and 4. The relative efficiency of the detection setup was determined using the previously measured angular distributions [4,20,22] of the $E_p = 1210$ keV resonance of the $^{15}\mathrm{N}(p,\alpha_1\gamma)\,^{12}\mathrm{C}^*$ reaction.

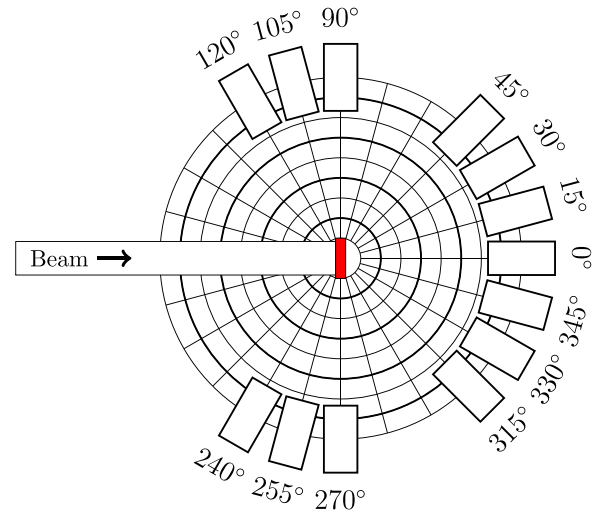

FIG. 3. Diagram of the experimental setup, which consisted of 13 $LaBr_3$(Ce) detectors from the HAGRiD array, used to measure the angular distributions of the $E_\gamma = 4.44$ MeV secondary γ-ray from the $^{15}\mathrm{N}(p,\alpha_1\gamma)\,^{12}\mathrm{C}^*$ reaction.

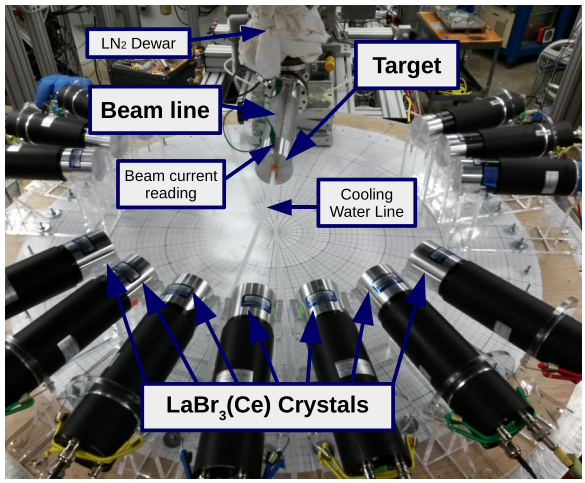

FIG. 4. Photograph of the setup used for the present measurement.

The HAGRiD $LaBr_3$(Ce) detectors are ideally suited for these measurements of the $E_\gamma = 4.44$ MeV γ-ray for a number of reasons. The γ-ray energy is well above the intrinsic background of the detector, which ends at $E_\gamma \approx 3.5$ MeV as shown in Fig. 5. Compared to a high-purity germanium (HPGe) detector of the same physical dimensions, a $LaBr_3$(Ce) detector is significantly more efficient [28], and thanks to the absence of nearby γ-rays in this measurement, the excellent energy resolution of an HPGe detector is not required. An example γ-ray energy spectrum is shown in Fig. 5 for a proton beam energy of $E_p = 3.900$ MeV. No appreciable intrinsic or environmental background was observed in the region of interest.

The data acquisition system consisted of two CAEN N6730 digitizers (500 MS/s, 14 bit) equipped with CAEN DPP-PSD firmware. The readout and board parameter setup was performed using the software CoMPASS, freely available from CAEN. Using the built-in USB 2.0 connection data were acquired directly from digitizers in "list mode" recording outputs (short integral, long integral, and time stamp) provided by the DPP-PSD firmware. The onboard FPGA waveform processing and the fast $LaBr_3$(Ce) signals provided for fast data acquisition resulting in measurements virtually free of dead time.

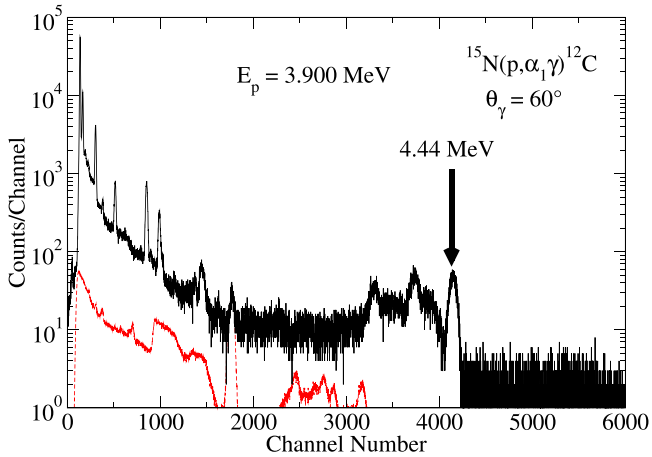

FIG. 5. Example γ-ray spectrum from one of the $LaBr_3$(Ce) HAGRiD detectors used in the present measurement (solid black line) and a normalized background spectrum (dashed red line). The γ-ray line at $E_\gamma = 4.44$ MeV is clearly visible and is at an energy well above the intrinsic background of the detectors. The full-energy γ-ray peak was used to determine the cross section of the $^{15}\mathrm{N}(p,\alpha_1\gamma)\,^{12}\mathrm{C}^*$ reaction.

A total of 13 HAGRiD detectors were used for the measurement. The detectors were placed in a symmetric "east-west" configuration, giving seven unique angles of measurement that correspond to effective angles of 0 to 90° in steps of 15°. The setup results in each angle being measured twice in a symmetric pattern relative to the beam, except at 0°. The final cross sections are the geometric mean of the efficiency-corrected mirrored detectors, resulting in cancellation of asymmetries due to shifts in the beam spot position. Since secondary γ-ray angular distributions are symmetric about 90° as discussed in Sec. II, both forward and backward angles were utilized to optimize the setup to reduce γ-ray attenuation through the target holder and beam pipe.

Since the efficiency-corrected differential yields $\frac{dY}{d\Omega}$ show slow variations as a function of the energy compared to the energy loss of the beam through the target ($\Delta E_{\mathrm{target}}$), a thin target approximation is adopted [$\frac{d\sigma}{d\Omega}(E_{\mathrm{eff}},\theta_\gamma) \approx \frac{dY}{d\Omega}(E_{\mathrm{eff}},\theta_\gamma)$]. The differential yield is obtained from the number of counts in the full energy γ-ray peak $\frac{dA}{d\Omega}$ by

$$\frac{dY}{d\Omega}(E_{\mathrm{eff}},\theta_\gamma) = \frac{\frac{dA}{d\Omega}(E_p,\theta_\gamma)}{N_p(E_p)N_t\epsilon(E_\gamma,\theta_\gamma)}, \tag{8}$$

where N_p is the number of protons impinged on the target for a given proton energy, N_t is the target thickness (taken to be constant throughout the measurements), and $\epsilon(E_\gamma,\theta_\gamma)$ is the detection efficiency for an $E_\gamma = 4.44$ MeV γ-ray for a given detector at an angle θ_γ relative to the incident proton beam. The effective energy of the measurements (E_{eff}) is taken as $E_{\mathrm{eff}} = E_p - \frac{1}{2}\Delta E_{\mathrm{target}}$, where the energy loss through the Ti ^{15}N target (E_{target}) was calculated with stopping powers from SRIM [29]. The absolute cross section was obtained by normalizing the present data to the angle-integrated data of Imbriani *et al.* [27] and to the consistent differential cross-section measurements by Bray *et al.* [4] at $E_p = 1.205$ MeV and by Kraus *et al.* [20] and Bashkin and Carlson [22] at $E_p = 1.21$ MeV (see Fig. 2). The absolute differential cross sections are shown in Fig. 2. Typical statistical uncertainties were ≈3%. The data are shown in Fig. 6 and are available in the Supplemental Material [30].

IV. PREVIOUS MEASUREMENTS

One rigorous test of the current understanding of the level structure of a compound system is the ability to achieve a global R-matrix fit for the experimental data that sample several different reaction pathways. The inclusion of differential cross-section data is key since they provide a great deal of additional constraint. For the ^{16}O system, a global R-matrix fit was achieved up to about $E_x = 13.75$ MeV by deBoer *et al.* [10], which was later expanded to perform an evaluation

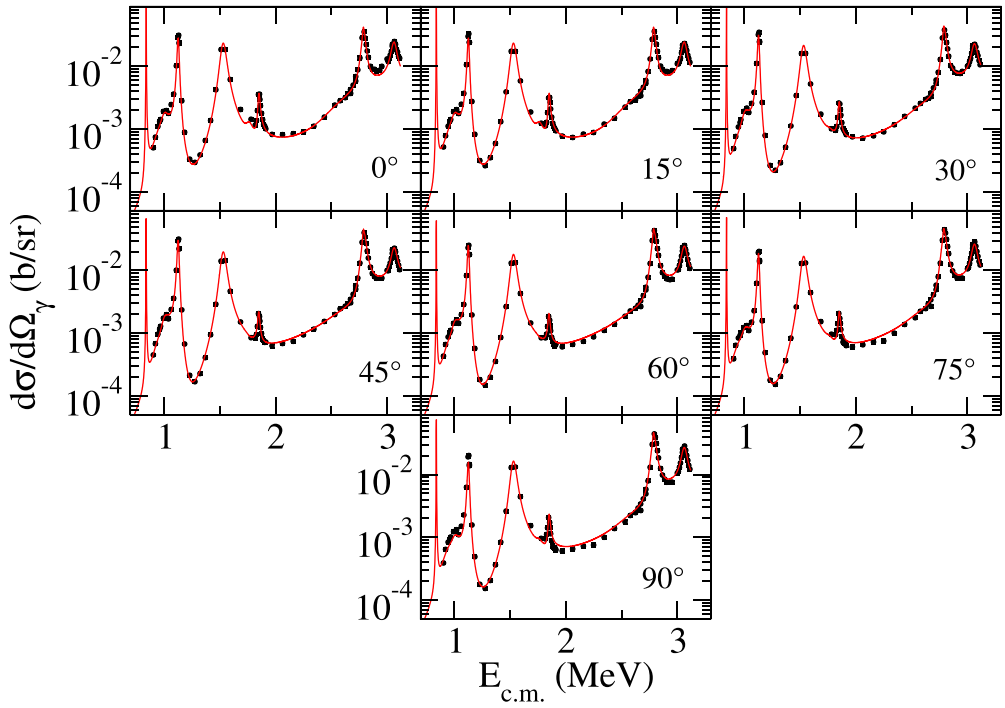

FIG. 6. The differential cross sections of the ^{15}N$(p,\alpha_1\gamma)\,^{12}$C* reaction from this work (see Sec. III). Uncertainties are usually smaller than the data point size and reflect only the statistical uncertainties. The red curve represents the *R*-matrix fit described in Sec. V.

of the ^{12}C$(\alpha,\gamma)\,^{16}$O reaction [16]. For that work, attempts were made to extend the fit to even higher energies, but this could not be achieved and no results were reported. Here the difficulties that were encountered are discussed in light of the new measurements presented in Sec. III.

The extended energy range covers a proton laboratory energy from 1.62 MeV $< E_p <$ 3.35 MeV (1.52 MeV $< E_{\rm cm} <$ 3.14 MeV or 13.75 MeV $< E_x <$ 15.27 MeV). The high-energy range has been limited by the opening of additional reaction channels, in particular, those that can proceed by multiparticle breakup. Three and four α-particle breakup reactions [^{15}N$(p,2\alpha)\,^{8}$Be and ^{15}N$(p,3\alpha)\,^{4}$He] become energetically possible at $E_p = 2.56$ and 2.46 MeV ($E_x = 14.53$ and 14.43 MeV), respectively. When these reaction channels become significant in cross sections compared to the other reaction channels, the standard *R*-matrix formalism of Lane and Thomas [17] is no longer sufficient. Curtis *et al.* [31,32] observed these decays at higher energies in their measurements and did not find an appreciable yield below $E_x \approx 16$ MeV, so the assumption is made that over this energy range the formalism is still valid. For the present measurements, the neutron channel opens at $E_p = 3.77$ MeV ($E_x = 15.66$ MeV).

Complementing the current measurements are several studies using ^{12}C$+\alpha$ reactions, corresponding to an α-particle energy range of 8.75 MeV $< E_\alpha <$ 10.81 MeV in the laboratory frame (6.59 MeV $< E_{\rm cm} <$ 8.11 MeV). It is important to note that only natural parity states can be accessed by these reactions. Additionally, at these energies, higher incoming angular momenta may be readily accessed by the ^{12}C$+\alpha$ reactions but not accessible through the ^{15}N$+p$ reactions. This is seen most readily when comparing the ^{15}N$(p,\alpha_1)\,^{12}$C and ^{12}C$(\alpha,\alpha_1)\,^{12}$C reactions, where the reactions populate a largely different set of levels (see Table III and Fig. 7).

A. ^{15}N$(p,\alpha_1\gamma)\,^{12}$C*

Over the energy range of interest, the only previous measurement of the ^{15}N$(p,\alpha_1\gamma)\,^{12}$C* reaction (observing secondary γ-rays) was made by Bashkin and Carlson [22], which

TABLE II. Masses and particle separation energies used in the *R*-matrix calculation. The quantities S_α, S_p, and S_{α_1} represent the separation energies of an α particle, a proton, and an α particle with ^{12}C in its first excited state, respectively. Masses are in atomic mass units; channel radii, in fm. Masses and separation energies are taken from Audi *et al.* [52].

Parameter	Value
S_α	7.16192(1) MeV
S_p	12.12741(1) MeV
S_{α_1}	11.60083(31) MeV
m_p	1.00782503207(10)
m_α	4.00260325415(6)
$m(^{12}$C)	12
$m(^{15}$N)	15.00010889823(15)
$m(^{16}$N)	16.006101658(2815)
$m(^{16}$O)	15.99491461956(16)
a_α	5.43
a_p	5.03
a_{α_1}	5.43

TABLE III. Observable energies and particle widths for the *R*-matrix fit. Parameters in boldface were treated as fit parameters; the sign in front of the partial widths indicates the relative interference sign of the corresponding reduced width amplitude. The fit was not unique for the unnatural parity states, emphasizing the need for additional data that constrain these channels. Partial widths for a given particle partition are listed in order of the lowest orbital angular momentum or intrinsic spin where appropriate. Partial widths from the literature are those of the compilation [51]. The complete details of the fit can also be found in the AZURE2 input file, which is provided in the Supplemental Material [30]. The parameters of lower energy levels were fixed to the values presented by deBoer *et al.* [16].

J^π	$\tilde{E}_x$ (MeV)		keV				
			$\tilde{\Gamma}_{\alpha_0}$:	$\tilde{\Gamma}_{p_0}$:	$\tilde{\Gamma}_{\alpha_1}$:	$\tilde{\Gamma}$	
	This work	Lit. [51]	This work	This work	This work	This work	Lit. [51]
0^+	**13.6146**	14.032(15)[a]	**1.92 x 10^3**	**3.36**	**−3.40**	1.92×10^3	185(35)
1^+	**13.6604**	13.664(3)		**0.0/−14.4**	**50.9**	65.3	64(3)
4^+	**13.8738**	13.869(2)	**56.7**	**−38.8 x 10^{-3}**	**−20.6**	77.3	89(2)
2^-	**13.9793**	13.980(2)		**0.143/-0.0947**	**20.8**	20.9	20(2)
$4^{(-)}$[b]	14.302(3)						34(12)
5^+[b]	14.399(2)						27(5)
4^+	**14.5131**	14.62(2)[c]	**266**	**0.057**	**270**	536	490(15)
5^-	**14.5771**	14.660(20)	**635**	**−0.69 x 10^{-3}**	**4.35**	639	670(15)
0^+	**14.6708**	—[a]	**−1.96 x 10^3**	**−33.2**	**−6.40**	1.99×10^3	
6^+	**14.8189**	14.8153(16)	**21.6**	**−5.84 x 10^{-3}**	**24.5/1.45**	63	70(8)
3^-	**14.8778**	14.10(10)	**−124**	**1.31**	**58.8/−370**	554	750(200)
(1^+)[d]	**14.9148**			**30.8/−0.230**	**28.0**	60.0	
2^+	**14.9210**	14.926(2)	**26.7**	**15.6**	**0.789/−20.3**	63.4	54(5)
4^+	**14.9404**	—[c]	**139**	**0.606**	**−2.37 x 10^3**	2.50×10^3	
(2^-)[d]	**14.9911**			**67.7 x 10^{-3}/−4.53**	**64.7/80.3**	150	
2^-	**15.1843**	15.196(3)		**−37.6/−6.60**	**−4.96/16.4**	65.6	63(4)
0^+	**15.2622**	15.097(5)	**−1.10 x 10^3**	**−11.4**	**93.6**	1.20×10^3	166(30)
2^+	**15.4348**	15.260(50)	**3.48 x 10^3**	**4.07**	**2.53/0.888**	3.48×10^3	300(100)
3^-	**15.4421**	15.408(2)	**116**	**−10.8**	**−74.6**	201	132(7)
1^-	**15.5037**	Background	**498**	**11.6/−30.1**	**−419/−192**		
1^+	**15.6508**	Background		**875/−166**	**31 x 10^{-3}**		
5^-	**15.863**	Background	**290**	**−0.611**	**−604**		
3^+	**15.9524**	Background		**407/0.550**	**−64.2**		
3^-	**16.0408**	Background	**89.7**	**21.7**	**26.1**		
3^+	**16.3607**	Background		**1.33 x 10^3/388**	**78.7/1.16**		
1^-	**16.4266**	Background	**−206**	**−1.12 x 10^3/972**	**538/504**		
6^+	**16.9082**	Background	**1.50 x 10^3**	**−0.558**	**1.89 x 10^3**		
2^+	**36.776**	Background	**12.5 x 10^3**	**−54.4 x 10^3**	**5.24 x 10^3/ − 76.0**		
0^+	40	Background	**−93.2 x 10^3**				
1^-	40	Background	**109 x 10^3**				
2^+	40	Background	**−108 x 10^3**				
3^-	40	Background	**−146 x 10^3**				
4^+	40	Background	**238 x 10^3**				
5^-	40	Background	**199 x 10^3**				

[a]The apparent single narrower [$\Gamma = 185(35)$ keV] 0^+ level reported by Tilley *et al.* [51] at $E_x = 14.032(15)$ MeV has been found to be the result of interference between the two broad 0^+ levels reported here, at $E_x = 13.61$ and 14.67 MeV.

[b]These levels were not observed in the data.

[c]The apparent single 4^+ level [$\Gamma = 490(15)$ keV] previously reported at $E_x = 14.60(20)$ MeV was found to result from two broader 4^+ levels at $E_x = 14.51$ ($\Gamma = 536$ keV) and 14.94 MeV ($\Gamma = 2.50$ MeV).

[d]Additional unnatural parity states are likely present in this region, but the present data do not provide a unique determination of their spin parities.

includes an unnormalized excitation function at $\theta_\gamma = 0^\circ$ and angular distribution measurements at eight proton beam energies that correspond to the prominent peaks of observed resonances. The present measurements are in generally good agreement with those by Bashkin and Carlson [22], although it is noted that the angular distributions do require an angular attenuation correction (see Sec. II B, Table I).

B. ^{15}N$(p, \alpha_1)^{12}$C*

In addition to measurements of secondary γ-rays, the ^{15}N$(p, \alpha_1)^{12}$C reaction has been measured through detection of prompt α-particles by Bashkin *et al.* [33] and Frawley *et al.* [9]. Bashkin *et al.* [33] made comprehensive cross-section measurements at $\theta_{cm} = 86.2^\circ$ and 159.5° and

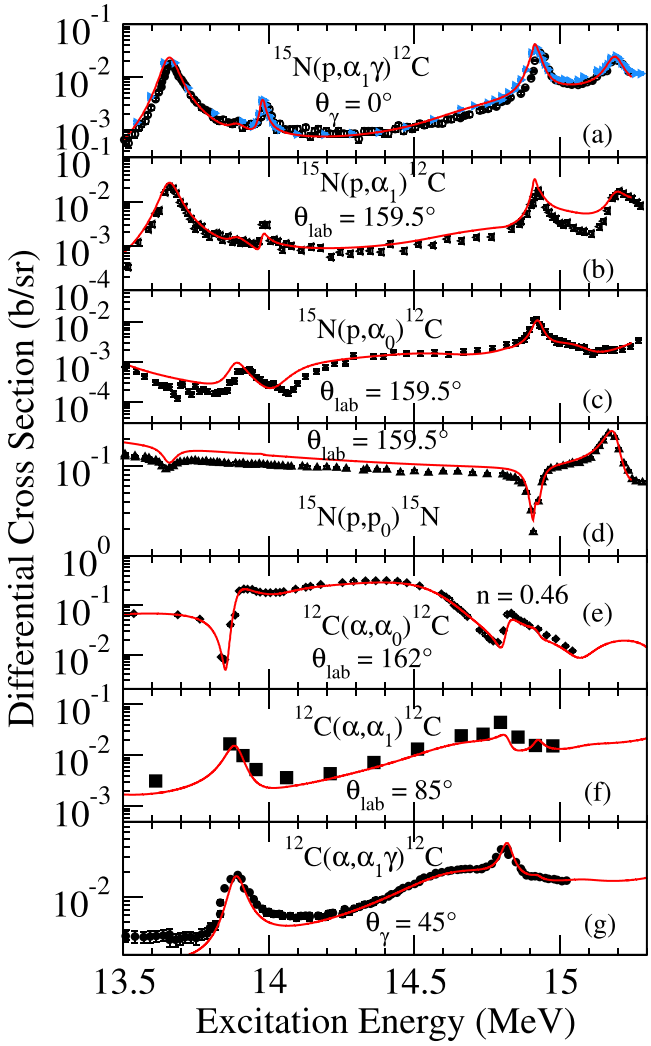

FIG. 7. A sample of data for each reaction channel where measurements exist over the excitation energy range of interest. The data in each subplot are as follows: (a) this work (blue triangles) and Bashkin and Carlson [22], (b–d) Bashkin *et al.* [33], (e, f) Ophel *et al.* [37], and (g) Larson and Spear [49]. The solid red line in (a)–(d), (f), and (g) indicates the best fit, obtaining the parameters given in Table III. Note that the data in (e) have been renormalized as discussed in Sec. V A (see Fig. 10). The differential cross sections are in the center-of-mass frame.

measured angular distributions at six on-resonance energies. The measurements by Frawley *et al.* [9] concentrated on making detailed differential cross-section measurements over the more limited energy range from $E_p = 2.88$ to 3.64 MeV, where several closely spaced resonances were observed by Bashkin *et al.* [33]. Jausel-Hüsken and Freiesleben [34] also measured over this higher-energy region at $\theta_{\rm lab} = 120^\circ$ and 150° from $E_p = 2.5$ MeV to $E_p = 5.5$ MeV and give an angular distribution at $E_p = 2.99$ MeV. New measurements are under way by Swartz *et al.* [35].

C. ^{15}N(p, α_0)^{12}C

Frawley *et al.* [9] measured over the limited energy range from 2.88 MeV $< E_p <$ 3.64 MeV in roughly 40-keV steps and sampled at 16 different angles between $\theta_{\rm cm} = 25^\circ$ and $\theta_{\rm cm} = 170^\circ$. Bashkin *et al.* [33] measured differential cross sections at $\theta_{\rm lab} = 86.2^\circ$ and 159.5° as well as angular distributions at six on-resonance energies. Preliminary new measurements have been reported by Swartz *et al.* [35].

D. ^{15}N(p, p)^{15}N

Likewise, proton scattering studies that overlap this energy range are those by Bashkin *et al.* [33], which cover a wide energy range, and Frawley *et al.* [9], which concentrate on the higher-energy resonance region. Bashkin *et al.* [33] made their comprehensive cross-section measurements at $\theta_{\rm cm} = 90^\circ$ and 160.8° and measured angular distributions at seven on-resonance energies. Darden *et al.* [36] measured detailed excitation functions at $\theta_{\rm cm} = 98.8^\circ$ and 156.6° from 2.7 MeV $< E_p <$ 7.0 MeV and measured four angular distributions over the energy range of interest. Jausel-Hüsken and Freiesleben [34] measured excitation functions at $\theta_{\rm lab} = 120^\circ$ and 150° from $E_p = 2.5$ MeV to $E_p = 5.5$ MeV.

E. ^{12}C(α, α)^{12}C

Several measurements of the ^{12}C$(\alpha, \alpha)^{12}$C reaction have been made over this energy range. Ophel *et al.* [37] made detailed measurements from $E_x = 13.5$ MeV to $E_x =$ 15.0 MeV, improving on the earlier measurements by Ferguson and McCallum [38] and Carter *et al.* [39]. Marvin and Singh [40] published additional measurements but with poorer resolution and larger uncertainties than Ophel *et al.* [37]. Three angular distributions measurements were also made earlier by Brady *et al.* [41]. A phase-shift analysis was performed by Ophel *et al.* [37] but a consistent description of the differential cross section could not be achieved. The analysis was improved on by Martin and Ophel [42], who performed limited *R*-matrix fits, which resulted in improvement, but still could not find a satisfactory description of the data. Targeted measurements of the lowest-energy 6^+ state in ^{16}O were made at energies around $E_x = 14.79$ MeV by Ophel *et al.* [43] and Ramirez and Bernstein [44]. More recently, measurements for IBA applications were made by Banks *et al.* [45], and thick target inverse kinematics measurements by Ashwood *et al.* [46]. It should also be noted that there is a very comprehensive measurement by Ames [47], but their measurements only overlap at the highest energies investigated here.

F. ^{12}C(α, α_1)^{12}C*

The only measurements of the ^{12}C$(\alpha, \alpha_1)^{12}$C reaction (primary particle detected) over this energy range are by Mitchell *et al.* [48] and Ophel *et al.* [37]. Mitchell *et al.* [48] made measurements from 9.5 MeV $< E_\alpha <$ 19 MeV, but only measured over the present region of interest at the four forward angles of $\theta_{\rm lab} = 54.5^\circ$, 71.5°, 90°, and 106.5°. Ophel *et al.* [37] reports 15 detailed angular distributions from 8.3 MeV $< E_\alpha <$ 10.42 MeV.

G. $^{12}C(\alpha, \alpha_1\gamma)^{12}C^*$

Measurements of the $^{12}C(\alpha, \alpha_1\gamma)^{12}C$ cross section have been made by Ophel *et al.* [37] and Mitchell *et al.* [48]. Ophel *et al.* [37] measured angular distributions but only reported the coefficients. Mitchell *et al.* [48] give an excitation function covering the wide energy range from 6 MeV $< E_\alpha <$ 17 MeV and measured four on-resonance angular distributions over the energy range of interest. Larson and Spear [49] report an unnormalized excitation function measured at $\theta_\gamma = 45^\circ$ from 7.5 MeV $< E_\alpha <$ 10.5 MeV.

V. *R*-MATRIX ANALYSIS

In this section, the *R*-matrix fit of deBoer *et al.* [16] is extended from $E_x \approx 13.75$ MeV up to $E_x \approx 15$ MeV, with a focus on the new $^{15}N(p, \alpha_1\gamma)^{12}C^*$ data presented in Sec. III. This analysis seeks to combine the previous $^{12}C+\alpha$ and $^{15}N+p$ analyses by Martin and Ophel [42] and Frawley *et al.* [9], respectively, in order to achieve a more consistent *R*-matrix analysis over this excitation energy region. As such, these data are the focus of the comparison, however, many of the data discussed in Sec. IV are also included in the global *R*-matrix fit.

As by deBoer *et al.* [16], the *R*-matrix fit uses the alternative parametrization of Brune [50] to work directly with observed energies and partial widths. The adopted values for the masses and separation energies are given in Table II. Over this higher-energy region, several higher-energy levels beyond those of deBoer *et al.* [16] are accessed and were added to the analysis (see Table III). The formalism summarized in Sec. II and derived by Brune and deBoer [1] is used to fit secondary γ-ray differential cross-section data for the $^{15}N(p, \alpha_1\gamma)^{12}C^*$ and $^{12}C(\alpha, \alpha_1\gamma)^{12}C$ reactions. It should also be noted that the γ-ray decay from the first excited state of ^{12}C to the ground state is a pure $E2$ transition [51].

As this section focuses on the multi-entrance-channel aspects of the *R*-matrix fit, excitation energies are used to discuss the resonance placement. To aid in these discussions, Fig. 7 shows a sampling of data sets for each reaction pathway plotted versus the excitation energy.

A reasonably consistent fit was obtained for the global fitting, especially for the $^{12}C(\alpha, \alpha_0)^{12}C$ data, but difficulties were encountered in fitting the $^{15}N+p$ data. This is largely attributed to the lack of data for these reactions. While the present measurements are a significant improvement in the energy and angular coverage for the $^{15}N(p, \alpha_1\gamma)^{12}C^*$ differential cross section, available $^{15}N(p, \alpha_0)^{12}C$, $^{15}N(p, \alpha_1)^{12}C^*$, and $^{12}C(\alpha, \alpha_1)^{12}C^*$ data remain scarce.

Several strategies were attempted to achieve the best global fit. In the end, the best fit was found by first obtaining a good fit to the $^{12}C(\alpha, \alpha_0)^{12}C$ data, thereby constraining the level parameters of the broad natural parity states. Then the fit was extended to the $^{15}N(p, \alpha_0)^{12}C$ and $^{12}C(\alpha, \alpha_1)^{12}C$ data, and finally, the fit was extended again to include the $^{15}N(p, p)^{15}N$ and $^{15}N(p, \alpha_1)^{12}C^*$ data.

The *R*-matrix fit also contains a rather large number of background levels as listed in Table III. While it is reasonable to investigate at least one additional background level per J^π, analyses of lower-energy data often find that only a few have an impact on the fit. In general, there are two main reasons that background levels are justifiable in phenomenological *R*-matrix theory. The first is that there may be one or more additional levels present just above the highest energy of the data under consideration that are broad enough to affect the cross section over the region of the data. The second is to mimic a reaction direct mechanism component.

In this work, as in previous *R*-matrix analyses of the $^{12}C(\alpha, \alpha)^{12}C$ reaction [10,16,53–55] even at lower energies, background levels with large α-particle widths, where the other partial widths are constrained to be 0, are needed to describe the experimental $^{12}C(\alpha, \alpha)^{12}C$ data. The need for these background levels is attributed, at least in part, to a weak direct component. In addition, for this higher-energy fit, it was found that an additional set of background levels was needed to compensate for higher-energy levels that are just above the region of the data investigated here. These background levels were allowed to have nonzero partial widths in all relevant channels. Several attempts were made to decrease the number of these background levels, but all were found to make significant contributions to the fit. This added complexity compared to fits at lower energies is attributed to the increasing level density over this higher-energy region.

The excitation energies for previously reported levels obtained in this work are often different from those reported in the compilation [51]. For consistency and ease of reference, the energies of the compilations are always used, except when specifically stated otherwise. Table III summarizes the differences in the level energies obtained in the present work versus those given in the compilation [51].

A. $^{12}C(\alpha, \alpha_0)^{12}C$

A good fit to the $^{12}C(\alpha, \alpha_0)^{12}C$ data is highly desirable since these data place strong constraints on the broad natural parity states that are present throughout this region. This is further facilitated by the fact that the α-scattering cross-section measurements are the most comprehensive of any of the reactions measured over this excitation energy region. An *R*-matrix fit of the α-scattering data over this region was attempted previously by Martin and Ophel [42], but their analysis was limited, by practical constraints of the time, to a single level approximation (per J^π). It has been found, as detailed in Table III, that this was an insufficient approximation, and it is clearly the reason they were unable to obtain a good fit to their data.

The compilation [51] lists several natural parity states over this excitation energy range, many of which are clearly present in the scattering data. In particular, the narrow 4^+ level at $E_x = 13.87$ MeV, the broad 5^- level at $E_x = 14.66$ MeV, and the narrower 6^+ level at $E_x = 14.85$ MeV are quite prominent. However, these levels alone are insufficient to describe the scattering cross section. The broad 5^- level alone is unable to completely reproduce the prominent resonance structure near $E_x = 14.66$ MeV, and in addition, it is verified that the broad 3^-, 4^+, and 2^+ levels that have previously been reported at $E_x = 14.10$, 14.62, and 15.26 MeV [51] are required. With these additional broad levels, the cross section

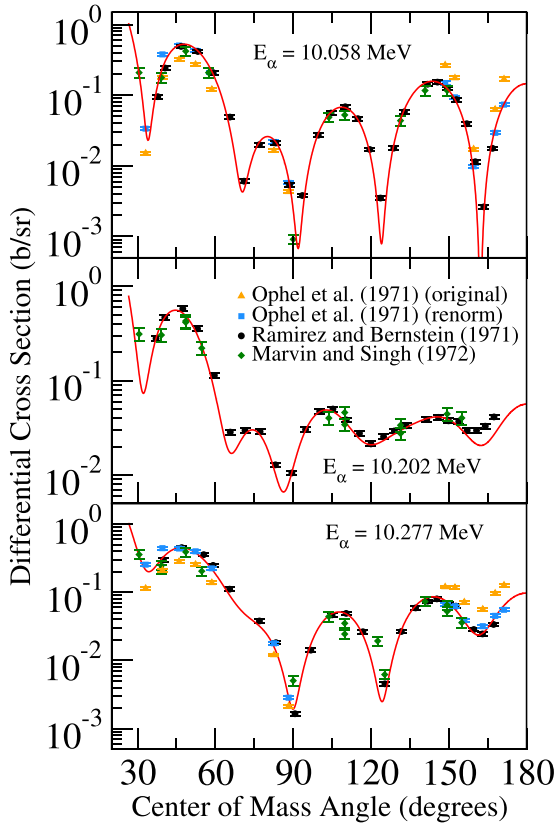

FIG. 8. Comparison of differential cross-section measurements for the ^{12}C$(\alpha,\alpha_0)^{12}$C reaction from Ramirez and Bernstein [44] (black circles), Marvin and Singh [40] (green diamonds), and Ophel *et al.* [37] (orange triangles, original data; blue squares, renormalized data) in the vicinity of the first $J^\pi = 6^+$ level in ^{16}O. The global *R*-matrix fit from the present work is also shown (red line). Renormalization of the data of Ophel *et al.* [37] was done for each angle, as shown in Fig. 10. The differential cross sections are in the center-of-mass frame.

below the 4^+ level at $E_x = 13.87$ MeV and in the vicinity of the 5^- level at $E_x = 14.66$ MeV and the narrower 6^+ level at $E_x = 14.85$ MeV could be reproduced quite well. However, in the intermediate-energy range, large discrepancies remained.

The compilation [51] lists a 0^+ level at $E_x = 14.032(15)$ MeV, but it was found that this level alone could not reproduce the data. Instead, it was found that two broad 0^+ levels were needed at $E_x = 13.61$ and 14.67 MeV, which strongly interference with each other, and the other broad resonances in the region. This gave an excellent reproduction of the cross section up to $E_x = 14.8$ MeV.

It should be noted that achieving the fit to the ^{12}C$(\alpha,\alpha_0)^{12}$C data was greatly hindered by errors in the reported normalizations of the data of Ophel *et al.* [37] and Martin and Ophel [42]. This issue was finally discovered through comparisons to the data of Marvin and Singh [40] and Ramirez and Bernstein [44], as shown in Fig. 8. The R-matrix fit is compared with the data of Marvin and Singh [40] in Fig. 9. It was found that at backward angles, the data of Ophel *et al.* [37] had to be multiplied by a factor of ≈ 0.5, while at forward angles, the factor was between 1.3 and 2.3. The reason for this discrepancy remains unknown. The normalization factors are given in Fig. 10.

The fit was then further extended up to $E_x = 15.5$ MeV, just above the neutron separation energy in ^{16}O ($S_n = 15.66$ MeV). Over this region, the α-scattering cross section is dominated by just two levels, the 0^+ at 15.097(5) MeV, the 2^+ at $E_x = 15.260(50)$, and the 3^- at $E_x = 15.408(2)$ MeV. However, it should be noted that the total widths of the 0^+ and 2^+ levels are much larger than those previously reported [51].

Finally, it is noteworthy that the prominent 2^+ level that appears in the ^{15}N$(p,\alpha_0)^{16}$O, ^{15}N$(p,\alpha_1)^{16}$O, and ^{15}N$(p,p)^{15}$N data makes no significant contribution to the α-scattering cross section. This is unfortunate, as it would be useful to have further constraints on the level properties of this state through this reaction. Discussions concerning this level are continued below and in Sec. VI.

B. ^{15}N$(p,\alpha_0)^{12}$C

As discussed in Sec. IV, there are very few measurements available for the ^{15}N$(p,\alpha_0)^{12}$C reaction over the energy range investigated in this work. The data of Bashkin *et al.* [33] cover the entire energy range of interest but are limited to a single angle ($\theta_{\rm lab} = 159.5^\circ$). While a satisfactory description of the differential cross section was obtained, data at only one angle make it likely that the solution is not unique. Conversely, the data of Frawley *et al.* [9] cover a wide angular range but are limited in energy. The reproduction of these data was not as good, which is attributed to the growing complexity of the level structure and the fact that these data are at the limits of the fit range. Again, the fit is not uniquely defined.

It should be noted that describing the weak resonance (corresponding to the prominent 4^+ level at $E_x = 13.869$ MeV in the ^{12}C$(\alpha,\alpha_0)^{12}$C data) at $E_p \approx 2.0$ MeV was very difficult when only the proton-induced data were considered. However, when combined with the fit to the ^{12}C$(\alpha,\alpha_0)^{12}$C data, a much better fit was obtained due to the additional constraint from those data. There is still a shift present in the location of the resonance, which is likely the result of somewhat inconsistent energy calibrations between the α-particle- and the proton-induced reaction data [see Fig. 7(c)]. The global fit is also compared to the data of Frawley *et al.* [9] in Fig. 11, which only cover the upper $E_{\rm c.m.} = 0.7$ MeV range of interest. In this channel, the cross section is dominated by an inference region between broad resonances and there is only one weak resonance at $E_{\rm c.m.} = 2.8$ MeV, which corresponds to the level(s) at $E_x = 14.92$ MeV (see Sec. VI).

C. ^{12}C$(\alpha,\alpha_1)^{12}$C*

Inelastic scattering measured via particle [37] and γ-ray [48,49] detection was included in the global fitting. For the secondary γ-ray data, those of Larson and Spear [49] cover a broad energy range, but due to difficulties in digitizing the data from figures in that work, low-cross-section regions likely have larger uncertainties than even those shown in Fig. 7(g). The angular distribution data of Mitchell *et al.* [48] also cover a wide energy range, although sampling only 11 energies (see

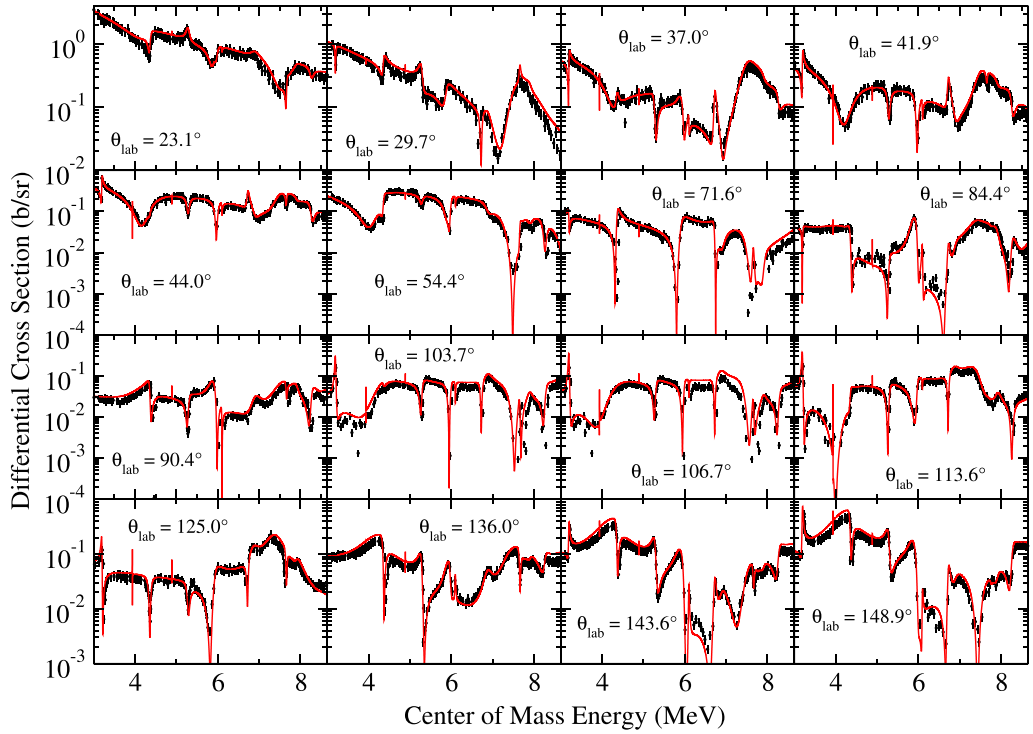

FIG. 9. *R*-matrix fit to the $^{12}C(\alpha,\alpha_0)^{12}C$ data of Marvin and Singh [40]. The differential cross sections are in the center-of-mass frame.

Fig. 12). Both data sets are well reproduced, although for the differential data, this may be partly due to the very similar γ-ray angular distributions that arise from the higher spin states (4^+, 5^-, and 6^+) owing to the limit placed on the maximum Legendre polynomial order ($L = 4$) by the multipolarity of the secondary γ-ray ($E2$).

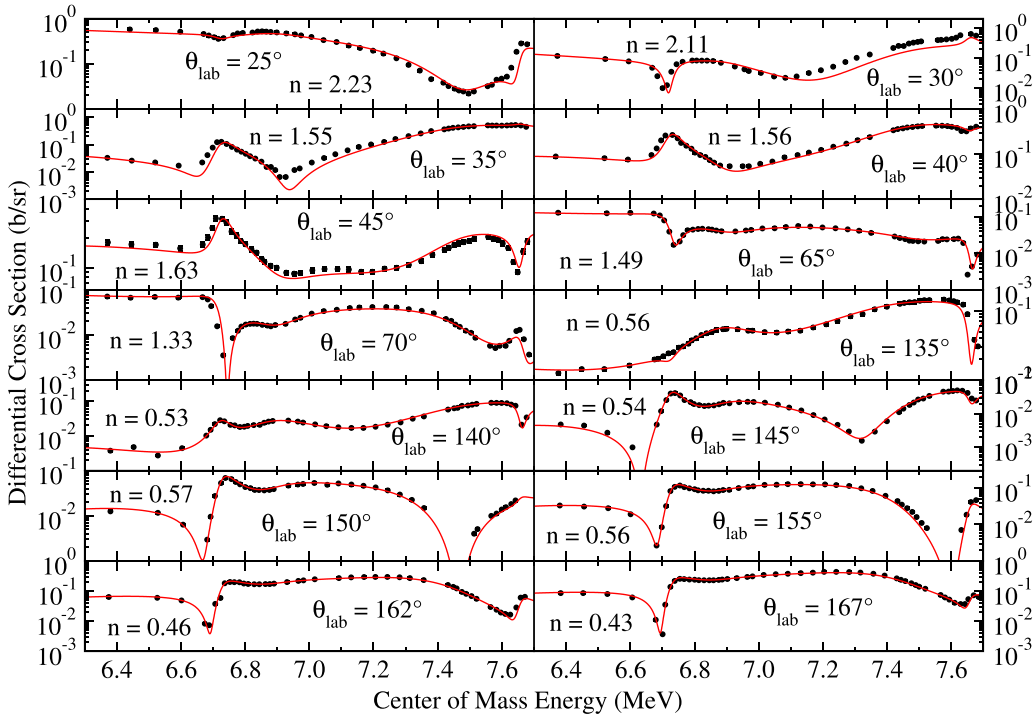

FIG. 10. Comparison of the global *R*-matrix fit to the $^{12}C(\alpha,\alpha_0)^{12}C$ data of Ophel *et al.* [37]. The differential cross sections are in the center-of-mass frame. The factors multiplied by the original data presented by Ophel *et al.* [37] (n) are discussed in Sec. V A.

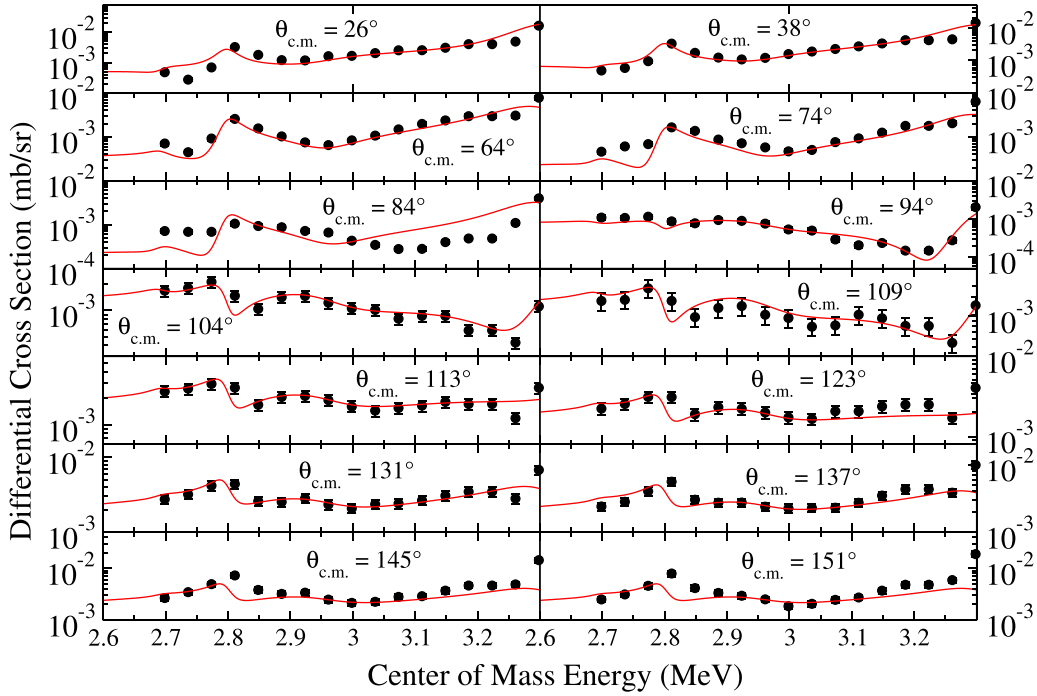

FIG. 11. Comparison of the present *R*-matrix fit to the ^{15}N$(p,\alpha_0)\,^{12}$C data of Frawley *et al.* [9]. The differential cross sections are in the center-of-mass frame. The quoted uncertainties are often smaller than the point size.

D. ^{15}N$(p,p)\,^{15}$N

Like the ^{15}N$(p,\alpha_0)\,^{12}$C data, the proton scattering data over this region are limited to the wide energy/limited angular coverage data of Bashkin *et al.* [33] and the wide angular coverage/limited energy range data of Frawley *et al.* [9]. The ^{15}N$(p,p)\,^{15}$N cross section is dominated by only two prominent resonances, which correspond to the 2^+ state at

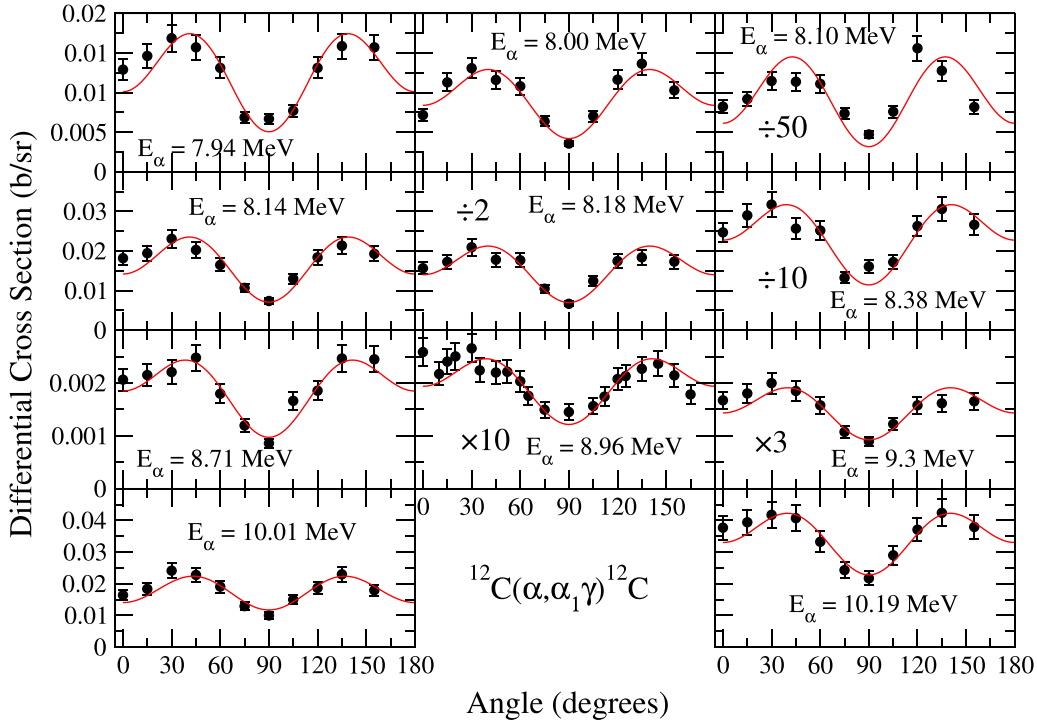

FIG. 12. Comparison of the present *R*-matrix fit to the ^{12}C$(\alpha,\alpha_1\gamma)\,^{12}$C* angular distribution data of Mitchell *et al.* [48] using the formalism of Brune and deBoer [1].

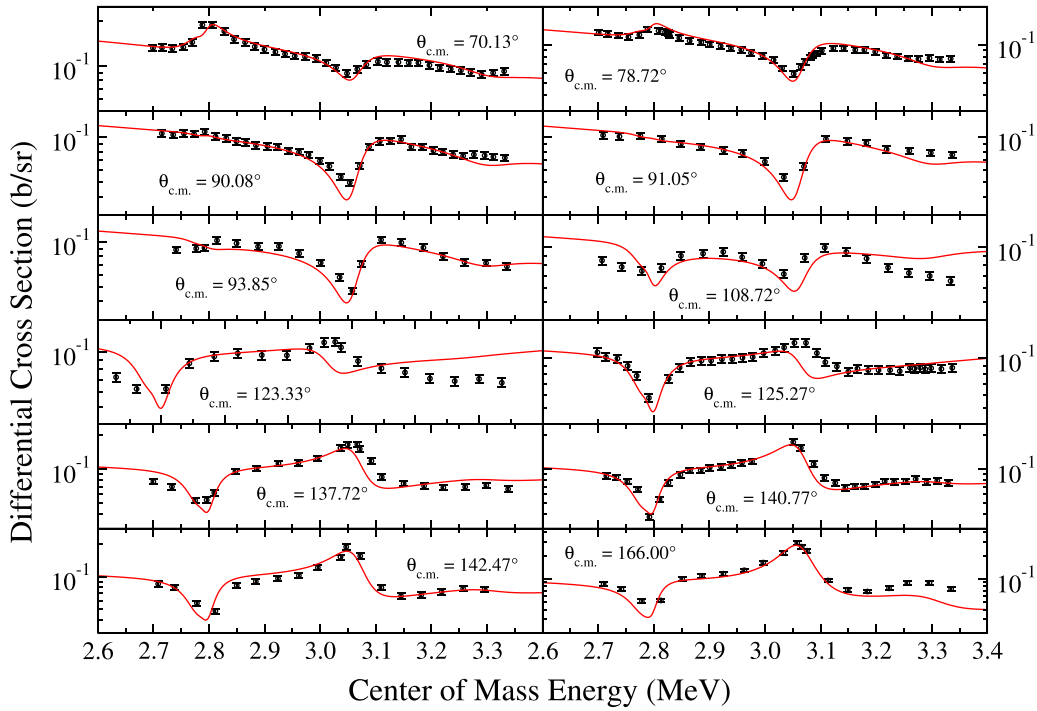

FIG. 13. Comparison of the global R-matrix fit to the $^{15}\mathrm{N}(p,p)^{15}\mathrm{N}$ data of Frawley *et al.* [9]. The differential cross sections are in the center-of-mass frame.

$E_x = 14.93$ and the 2^- state at $E_x = 15.20$ MeV. Only this reaction and the $^{15}\mathrm{N}(p,\alpha_1)^{12}\mathrm{C}$ reaction can populate unnatural parity states. The scarcity of unnatural parity states over this region is somewhat unexpected, and unidentified broad ones may be responsible for the difficulties in fitting the data. The global fit is compared to the data of Frawley *et al.* [9] in Fig. 13. As in [9], it was found that a broad 1^+ background level substantially improved the quality of the fit.

E. $^{15}\mathrm{N}(p,\alpha_1)^{12}\mathrm{C}^*$

There were major challenges encountered in obtaining a good fit to the $^{15}\mathrm{N}(p,\alpha_1)^{12}\mathrm{C}^*$ data, both that obtained from direct particle detection [9,33] and the present data using secondary γ-ray detection. In this work, a fair description of the present $^{15}\mathrm{N}(p,\alpha_1)^{12}\mathrm{C}^*$ data has been obtained at all angles of measurement, but significant discrepancies exist in the fit to the data of Frawley *et al.* [9] and Bashkin *et al.* [33]. In particular, it was difficult to find a consistent fit for the resonance at $E_{\mathrm{c.m.}} \approx 2.8$ MeV ($E_x = 14.92$ MeV) across all of the reaction channels. Additionally, the off-resonance data between the resonances at $E_{\mathrm{c.m.}} \approx 2.80$ and $E_{\mathrm{c.m.}} \approx 3.05$ MeV were quite difficult to reproduce. It seems likely that additional unnatural parity states exist in this region that have not yet been identified. To obtain the present fit, an additional 1^+ level was added very close to the 2^+ level at $E_x = 14.92$ MeV and an additional broad 2^- level was added in the off-resonance region as detailed in Table III. Further discussions are presented in Sec. VI. The global fit is compared to the data of Frawley *et al.* [9] in Fig. 14 and to the secondary γ-ray data of Bashkin and Carlson [22] and the present work in Fig. 15.

VI. DISCUSSION

As discussed in Sec. V E, it was particular difficult to accurately reproduce the experimental cross section in the vicinity of the resonance observed at $E^p_{\mathrm{c.m.}} \approx 2.8$ MeV ($E_x \approx 14.92$ MeV, $E^\alpha_{\mathrm{c.m.}} = 7.75$ MeV). The compilation [51] lists a single level in this region at $E_x = 14.926(2)$ MeV with $J^\pi = 2^+$. Preliminary fitting of only the proton-induced data over this energy range found that this level assignment gives a good fit to both the $^{15}\mathrm{N}(p,p)^{15}\mathrm{N}$ and the $^{15}\mathrm{N}(p,\alpha_0)^{12}\mathrm{C}$ data (as a function of both energy and angle), where this resonance is also clearly observed. However, a good fit could not be obtained for the $^{15}\mathrm{N}(p,\alpha_1)^{12}\mathrm{C}^*$ data, where neither the magnitude of the cross section nor the angular distribution of the data could be reproduced. Further, no resonance that corresponds to this level is observed in either the $^{12}\mathrm{C}(\alpha,\alpha_0)^{12}\mathrm{C}$ or the $^{12}\mathrm{C}(\alpha,\alpha_1)^{12}\mathrm{C}^*$ data, despite its being of natural parity. This seems to indicate that if this level is of natural parity, then it has a rather small α width.

With the above consideration, it seems likely that the observed resonance in the $^{15}\mathrm{N}(p,\alpha_1)^{12}\mathrm{C}^*$ reaction is in fact a doublet or has some very strong contribution from interference of additional levels with differing J^π. Many scenarios were considered. For a doublet, all J^π combinations up to $7^{(+/-)}$ were considered. No combination was found to be completely satisfactory, but $J^\pi = 1^+$ and 3^+ gave the best fits. One issue is that while a doublet can describe the

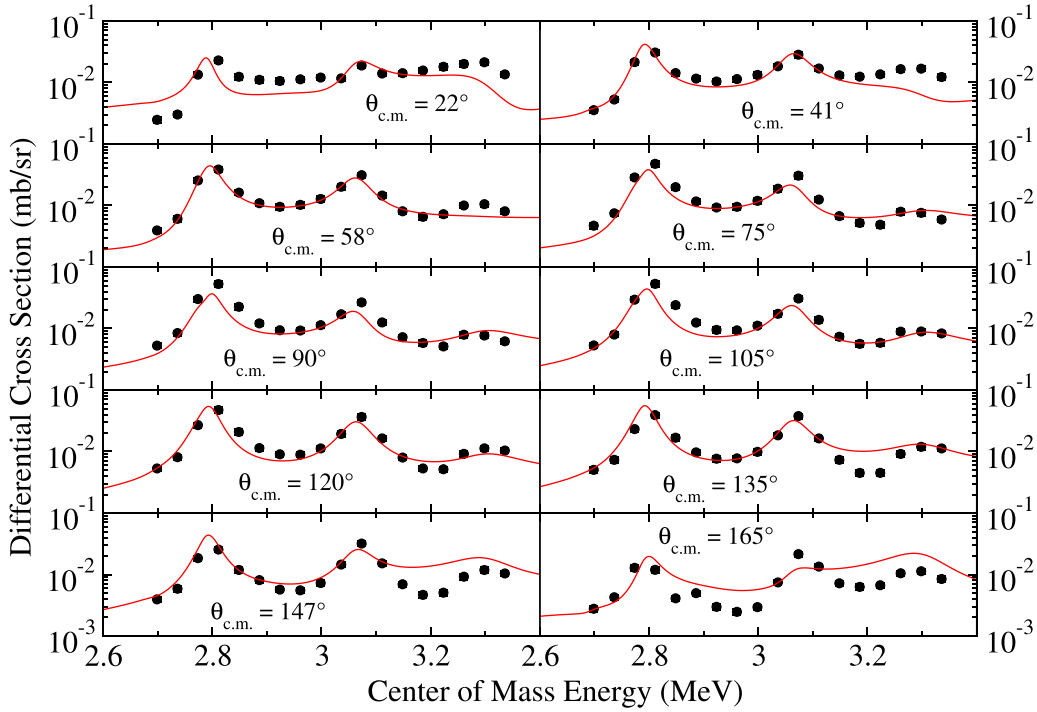

FIG. 14. Comparison of the global *R*-matrix fit to the $^{15}\mathrm{N}(p,\alpha_1)\,^{12}\mathrm{C}$ data of Frawley *et al.* [9]. The differential cross sections are in the center-of-mass frame.

$^{15}\mathrm{N}(p,\alpha_1)\,^{12}\mathrm{C}^*$ data well, it usually significantly worsened the fit to the $^{15}\mathrm{N}(p,p)\,^{15}\mathrm{N}$ data, which are described well by only the 2^+ level. Similarly, the $^{12}\mathrm{C}(\alpha,\alpha_0)\,^{12}\mathrm{C}$ data put significant constraints on the strength of any natural parity candidate. For example, considering only the $^{15}\mathrm{N}(p,\alpha_1)\,^{12}\mathrm{C}^*$ data, a combination of 2^+ and 1^- levels can describe the

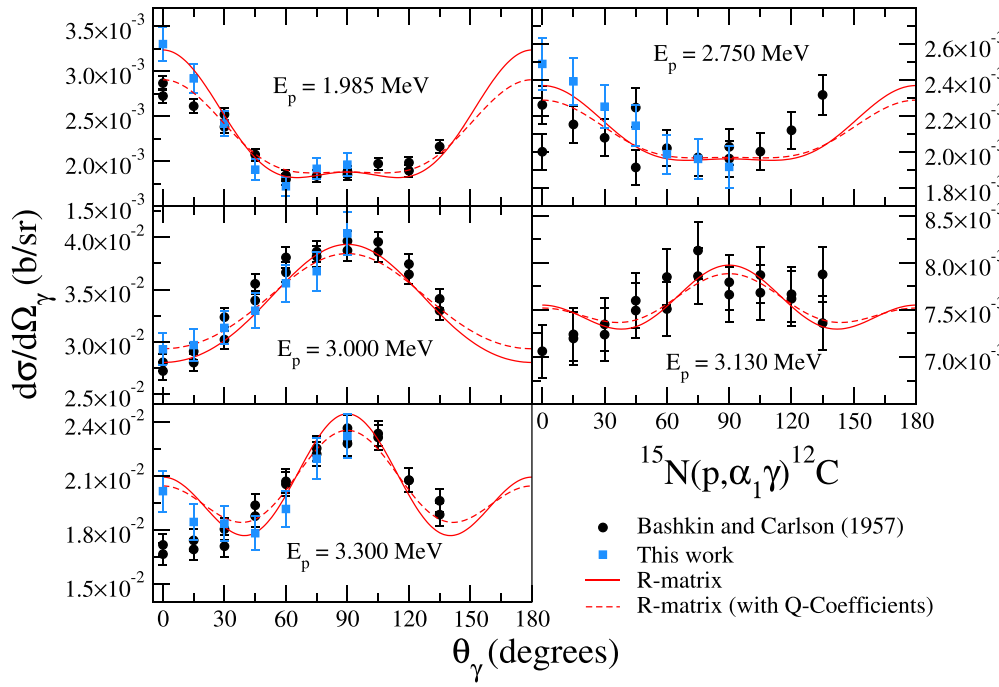

FIG. 15. Comparison of the global *R*-matrix fit to the data of Bashkin and Carlson [22] and that in this work at similar energies where available. Solid red lines indicate the bare *R*-matrix cross section, which should be compared with the present data, while dashed red lines are corrected for extended geometry and should be compared with the data of Bashkin and Carlson [22]. The *Q* coefficients for the data of Bashkin and Carlson [22] are listed in Table I.

cross section well, but this is then incompatible with the $^{12}C(\alpha,\alpha_0)^{12}C$ data.

Another possible solution is that the cross section over this region is enhanced due to the interference of two broad underlying levels, which both have level energies that are far from the apparent resonance. This seems to have been the solution found by Frawley *et al.* [9], where multiple broad ($\Gamma \approx 1$ MeV) levels cause an interference enhancement between them that mimics a resonance in this region. Frawley *et al.* [9] obtained their fit by introducing two broad 0^+ levels in addition to the reported 2^+ level. This is remarkably similar to the fit solution that was obtained for the $^{12}C(\alpha,\alpha_0)^{12}C$ data found in this work (see Sec. IV E). However, a similar solution could not be found that was compatible with the global fit of this work.

VII. SUMMARY

A comparison of past measurements of the $^{15}N(p,\alpha_1\gamma)^{12}C^*$ reaction has been made using the level parameters given in the *R*-matrix fit by deBoer *et al.* [16] and the mathematical formalism for secondary γ-ray angular distributions given by Brune and deBoer [1], and excellent agreement has been obtained. In addition, new higher-energy measurements of the $^{15}N(p,\alpha_1\gamma)^{12}C^*$ reaction, made at the University of Notre Dame using the HAGRiD array of $LaBr_3$(Ce) detectors, were performed in order to provide improved constraint on the level structure of ^{16}O up to $E_x \approx 15.3$ MeV. These measurements provide significantly improved energy/angular coverage of the differential cross section up to $E_p = 4.0$ MeV.

A global *R*-matrix fit was then performed, built on the lower-energy one of deBoer *et al.* [16], which includes both proton- and α-particle-induced reactions that populate the ^{16}O system. The analysis also built on, and combined, earlier, more limited *R*-matrix analyses by Frawley *et al.* [9] and Martin and Ophel [42]. While an excellent description of the $^{12}C(\alpha,\alpha)^{12}C$ and $^{15}N(p,\alpha_1\gamma)^{12}C^*$ cross sections was achieved, difficulties remain in describing the proton-induced data over certain energy and angular ranges. The difficulties in describing the proton-induced cross sections, and the success in describing the $^{12}C(\alpha,\alpha)^{12}C$ data, suggest that natural parity states over this region are well established, while some unnatural parity states have likely yet to be identified. The global *R*-matrix analysis presented here will be expanded in an upcoming work, where new data from a comprehensive new measurement of $^{12}C+\alpha$ data [56], similar to the previous lower-energy measurements by Tischhauser *et al.* [54], will be introduced.

ACKNOWLEDGMENTS

This research utilized resources from the Notre Dame Center for Research Computing and was supported by the National Science Foundation through Grant No. Phys-0758100 and the Joint Institute for Nuclear Astrophysics through Grant Nos. Phys-0822648 and PHY-1430152 (JINA Center for the Evolution of the Elements). The work at Ohio University was supported in part by the U.S. Department of Energy, under Grants No. DE-FG02-88ER40387 and No. DE-NA0003883. A portion of this work was supported by the U.S. Department of Energy under Grant No. DE-FG02-96ER40963 and the National Nuclear Security Administration under the Stewardship Science Academic Alliances program through DOE Cooperative Agreement DE-NA002132.

[1] C. R. Brune and R. J. deBoer, Phys. Rev. C **102**, 024628 (2020).
[2] R. E. Azuma, E. Uberseder, E. C. Simpson, C. R. Brune, H. Costantini, R. J. de Boer, J. Görres, M. Heil, P. J. LeBlanc, C. Ugalde, and M. Wiescher, Phys. Rev. C **81**, 045805 (2010).
[3] E. Uberseder and R. J. deBoer, *AZURE2User Manual* (Azure Biosystems, Dublin, CA, 2015).
[4] K. Bray, A. Frawley, T. Ophel, and F. Barker, Nucl. Phys. A **288**, 334 (1977).
[5] P. Dimitriou, R. J. DeBoer, S. Kunieda, H. Leeb, M. Paris, T. Srdinko, and I. J. Thompson, *Summary Report of Consultants' Meeting about "R-Matrix Codes for Charged-Particle reactions in the Resolved Resonance Region,"* Tech. Rep. INDC(NDS)-0703 (International Atomic Energy Agency, Vienna, Austria, 2016).
[6] H. Leeb, P. Dimitriou, and I.J. Thompson, *Summary Report of 2nd Consultants' Meeting about "R-Matrix Codes for Charged-Particle Reactions in the Resolved Resonance Region,"* Tech. Rep. INDC(NDS)-0726 (International Atomic Energy Agency, Vienna, Austria, 2017).
[7] H. Leeb, P. Dimitriou, and I.J. Thompson, *Summary Report of 3rd Consultants' Meeting about "R-Matrix Codes for Charged-Particle Reactions in the Resolved Resonance Region,"* Tech. Rep. INDC(NDS)-0737 (International Atomic Energy Agency, Vienna, Austria, 2017).
[8] H. Leeb, P. Dimitriou, and I.J. Thompson, *Summary Report of 4th Consultants' Meeting about "R-Matrix Codes for Charged-Particle Reactions in the Resolved Resonance Region,"* Tech. Rep. INDC(NDS)-0767 (International Atomic Energy Agency, Vienna, Austria, 2018).
[9] A. Frawley, K. Bray, and T. Ophel, Nucl. Phys. A **294**, 161 (1978).
[10] R. J. deBoer, J. Görres, G. Imbriani, P. J. LeBlanc, E. Uberseder, and M. Wiescher, Phys. Rev. C **87**, 015802 (2013).
[11] J.-P. Hirvonen, D. Rück, S. Yan, A. Mahiout, P. Torri, and J. Likonen, Surf. Coat. Technol. **74–75**, 760 (1995).
[12] S. Kumar, S. Vikram Kumar, G. Reddy, V. Kain, J. Ramana, and V. Raju, Nucl. Instrum. Methods Phys. Res. Sec. B **240**, 704 (2005).
[13] W. Lanford, Nucl. Instrum. Methods **149**, 1 (1978).
[14] J. Krauser, F. Wulf, and D. Bräunig, J. Non-Cryst. Solids **187**, 264 (1995).
[15] M. Wilde and K. Fukutani, Surf. Sci. Rep. **69**, 196 (2014).
[16] R. J. deBoer, J. Görres, M. Wiescher, R. E. Azuma, A. Best, C. R. Brune, C. E. Fields, S. Jones, M. Pignatari, D. Sayre, K.

Smith, F. X. Timmes, and E. Uberseder, Rev. Mod. Phys. **89**, 035007 (2017).
[17] A. M. Lane and R. G. Thomas, Rev. Mod. Phys. **30**, 257 (1958).
[18] G. R. Satchler, *Direct Nuclear Reactions* (Clarendon, Oxford, UK, 1983).
[19] H. J. Rose and D. M. Brink, Rev. Mod. Phys. **39**, 306 (1967).
[20] A. A. Kraus, A. P. French, W. A. Fowler, and C. C. Lauritsen, Phys. Rev. **89**, 299 (1953).
[21] C. A. Barnes, D. B. James, and G. C. Neilson, Can. J. Phys. **30**, 717 (1952).
[22] S. Bashkin and R. R. Carlson, Phys. Rev. **106**, 261 (1957).
[23] R. Leavitt, H. Evans, G. Ewan, H.-B. Mak, R. Azuma, C. Rolfs, and K. Jackson, Nucl. Phys. A **410**, 93 (1983).
[24] M. E. Rose, Phys. Rev. **91**, 610 (1953).
[25] M. S. Basunia, Nucl. Data Sheets **114**, 1189 (2013).
[26] P. J. LeBlanc, G. Imbriani, J. Görres, M. Junker, R. Azuma, M. Beard, D. Bemmerer, A. Best, C. Broggini, A. Caciolli, P. Corvisiero, H. Costantini, M. Couder, R. deBoer, Z. Elekes, S. Falahat, A. Formicola, Z. Fülöp, G. Gervino, A. Guglielmetti *et al.*, Phys. Rev. C **82**, 055804 (2010).
[27] G. Imbriani, R. J. deBoer, A. Best, M. Couder, G. Gervino, J. Görres, P. J. LeBlanc, H. Leiste, A. Lemut, E. Stech, F. Strieder, E. Uberseder, and M. Wiescher, Phys. Rev. C **85**, 065810 (2012).
[28] K. Smith, T. Baugher, S. Burcher, A. Carter, J. Cizewski, K. Chipps, M. Febbraro, R. Grzywacz, K. Jones, S. Munoz, S. Pain, S. Paulauskas, A. Ratkiewicz, K. Schmitt, C. Thornsberry, R. Toomey, D. Walter, and H. Willoughby, Nucl. Instrum. Methods Phys. Res. Sec. B **414**, 190 (2018).
[29] J. F. Ziegler and J. P. Biersack, *SRIM-2008, The Stopping and Range of Ions in Matter* (Nuclear Energy Agency of the OECD, Paris, 2008).
[30] See Supplemental Material at http://link.aps.org/supplemental/10.1103/PhysRevC.103.065801 for the experimental data and the AZURE2 input file from the *R*-matrix fit of this work.
[31] N. Curtis, S. Almaraz-Calderon, A. Aprahamian, N. I. Ashwood, M. Barr, B. Bucher, P. Copp, M. Couder, X. Fang, M. Freer, G. Goldring, F. Jung, S. R. Lesher, W. Lu, J. D. Malcolm, A. Roberts, W. P. Tan, C. Wheldon, and V. A. Ziman, Phys. Rev. C **88**, 064309 (2013).
[32] N. Curtis, S. Almaraz-Calderon, A. Aprahamian, N. I. Ashwood, M. Barr, B. Bucher, P. Copp, M. Couder, X. Fang, M. Freer, G. Goldring, F. Jung, S. R. Lesher, W. Lu, J. D. Malcolm, A. Roberts, W. P. Tan, C. Wheldon, and V. A. Ziman, Phys. Rev. C **94**, 034313 (2016).
[33] S. Bashkin, R. R. Carlson, and R. A. Douglas, Phys. Rev. **114**, 1543 (1959).
[34] S. Jausel-Hüsken and H. Freiesleben, Z. Phys. A **283**, 363 (1977).
[35] J. A. Swartz, H. O. U. Fynbo, K. L. Andersen, M. Munch, and O. S. Kirsebom, in *Proceedings of the 4th International Workshop on "State of the Art in Nuclear Cluster Physics" (SOTANCP4)*, edited by M. Barbui, C. M. Folden, III, V. Z. Goldberg, and G. V. Rogachev, AIP Conf. Proc. No. 2038 (AIP, New York, 2018), p. 020014.
[36] S. Darden, S. Sen, G. Murillo, M. Fernandez, J. Ramiez, A. Galindo, P. Jolivette, and B. Hichwa, Nucl. Phys. A **429**, 218 (1984).
[37] T. Ophel, P. Martin, S. Cloud, and J. Morris, Nucl. Phys. A **173**, 609 (1971).
[38] A. Ferguson and G. McCallum, Bull. Am. Phys. Soc. **6**, 235 (1961).
[39] E. B. Carter, G. E. Mitchell, and R. H. Davis, Phys. Rev. **133**, B1421 (1964).
[40] T. Marvin and P. Singh, Nucl. Phys. A **180**, 282 (1972).
[41] F. Brady, J. Jungerman, and J. Young, Nucl. Phys. A **98**, 241 (1967).
[42] P. Martin and T. Ophel, Nucl. Phys. A **202**, 257 (1973).
[43] T. Ophel, S. Cloud, P. Martin, and J. Morris, Phys. Lett. B **32**, 101 (1970).
[44] J. Ramirez and E. Bernstein, Nucl. Phys. A **173**, 207 (1971).
[45] J. C. Banks, W. R. Wampler, J. F. Browning, and B. L. Doyle, Nucl. Instrum. Methods Phys. Res. Sec. B **249**, 101 (2006).
[46] N. I. Ashwood, M. Freer, N. L. Achouri, T. R. Bloxham, W. N. Catford, N. Curtis, P. J. Haigh, C. W. Harlin, N. P. Patterson, D. L. Price, N. Soić, and J. S. Thomas, J. Phys. G: Nucl. Part. Phys. **36**, 055105 (2009).
[47] L. L. Ames, Phys. Rev. C **25**, 729 (1982).
[48] G. E. Mitchell, E. B. Carter, and R. H. Davis, Phys. Rev. **133**, B1434 (1964).
[49] J. Larson and R. Spear, Nucl. Phys. **56**, 497 (1964).
[50] C. R. Brune, Phys. Rev. C **66**, 044611 (2002).
[51] D. Tilley, H. Weller, and C. Cheves, Nucl. Phys. A **564**, 1 (1993).
[52] G. Audi, A. Wapstra, and C. Thibault, Nucl. Phys. A **729**, 337 (2003).
[53] P. Tischhauser, R. E. Azuma, L. Buchmann, R. Detwiler, U. Giesen, J. Görres, M. Heil, J. Hinnefeld, F. Käppeler, J. J. Kolata, H. Schatz, A. Shotter, E. Stech, S. Vouzoukas, and M. Wiescher, Phys. Rev. Lett. **88**, 072501 (2002).
[54] P. Tischhauser, A. Couture, R. Detwiler, J. Görres, C. Ugalde, E. Stech, M. Wiescher, M. Heil, F. Käppeler, R. E. Azuma, and L. Buchmann, Phys. Rev. C **79**, 055803 (2009).
[55] R. J. deBoer, A. Couture, R. Detwiler, J. Görres, P. Tischhauser, E. Uberseder, C. Ugalde, E. Stech, M. Wiescher, and R. E. Azuma, Phys. Rev. C **85**, 045804 (2012).
[56] R. deBoer, J. Görres, E. Stech, W. Tan, M. Wiescher, A. Long, K. Smith, and A. Boeltzig (unpublished).